Ultrafast thermalization of photoexcited carriers in polar semiconductors

Lucio Rota
Dipartimento di Fisica, Università di Modena, Via Campi 213/A, 41100 Modena, Italy

Paolo Lugli
Dipartimento di Ingegneria Elettronica, II. Università di Roma "Tor Vergata," Via della Ricerca Scientifico, 00173 Roma, Italy

Thomas Elsaesser
Physik Department E11, Technische Universität München, D-8046 Garching, Germany

Jagdeep Shah
AT&T Bell Laboratories, Holmdel, New Jersey 07733
(Received 24 August 1992)

We present a combined experimental and theoretical study of ultrafast thermalization of high-energy carriers photogenerated by femtosecond laser excitation in GaAs and InP. Luminescence up-conversion is used to monitor the spectral and temporal evolution of the carrier distribution with a time resolution of about 100 fs. A rapid redistribution of electrons and holes over a wide energy range is found within the first 100 fs after excitation. The experimental results are analyzed by Monte Carlo simulations including a molecular-dynamics scheme to describe the carrier kinetics. We show that the Coulomb interaction among carriers is responsible for the initial ultrafast thermalization.

I. INTRODUCTION

Femtosecond optical spectroscopy gives direct insight into the fundamental nonequilibrium properties of carriers, being able to monitor the fastest scattering processes of hot electrons and holes in semiconductors.[1–13] Monte Carlo (MC) simulations have been proven to be the most ideal theoretical tool for the study of such ultrafast processes, providing a one-to-one correspondence to the experimental situation.[10,14–17] Femtosecond excitation of III-V semiconductors like GaAs and InP generates an initial nonequilibrium distribution of electrons and holes, which thermalizes by carrier-carrier (CC) and longitudinal-optical (LO) phonon scattering to hot Fermi distributions. A subsequent slower relaxation towards equilibrium is controlled mainly by nonequilibrium phonon effects.[18–20]

For excitation 20 meV above the band gap, i.e., below the threshold of optical-phonon emission by the carriers, transient absorption spectra exhibit spectral holes.[4–6] Thermalization times of 50 up to 300 fs have been deduced from the data. For excitation of bulk GaAs at 2 eV, i.e., high above the band gap, the initial electron distribution consists of three peaks created by transitions from the heavy-hole, light-hole, and split-off valence band. The electrons not scattering to the L and X valleys equilibrate in the Γ valley. The transient decrease of absorption observed after femtosecond excitation reveals a spectral hole at 2 eV which disappears in tens of femtoseconds.[2,3] This kinetics is strongly influenced by intervalley scattering and cannot provide direct information about thermalization. The absorption change at energies far below 2 eV showed a rise within the temporal resolution of the experiments, which was interpreted as evidence for relaxation of electrons and holes on a time scale below 50 fs.[3] In contrast to this conclusion, recent MC simulations of these experiments suggest thermalization times of electrons of up to 300 fs and attribute the signals measured at low energies primarily to the faster equilibration of holes.[15] This discrepancy might be due (1) to the fact that in Ref. 3, no data were obtained below 1.57 eV and (2) to the difficulty in interpreting pump-probe experiments, where optical transitions from the heavy-hole, light-hole, and split-off valence band contribute to the observed transmission changes and the sum of the electron and hole distribution function, f_e+f_h, is measured. Either electrons or holes can cause bleaching, and carriers in different regions of the valence and conduction bands are monitored simultaneously at a specific probe wavelength. Therefore, unambiguous information on the electron distribution is difficult to extract from *absorption* studies. In contrast, the *luminescence* spectrum at energies below 1.7 eV is dominated by recombination with heavy holes. The emission intensity is proportional to the product $f_e f_h$, i.e., the presence of *both* electrons and heavy holes at the same k vector is necessary. Thus luminescence spectroscopy gives new independent information on the distribution of carriers.[10] Recently, continuous-wave hot luminescence has been used (and analyzed by MC simulations) to extract information on the scattering dynamics of high-energy electrons with a Fermi sea of cold electrons at the bottom of the conduction band, a situation which is quite different from the femtosecond experiments.[21,22] These studies of quasistationary carrier distributions have indicated equal low-temperature scattering times for electron-electron (EE) and electron-longitudinal-optical phonon interaction of 180 fs at a density of 8×10^{16} cm^{-3} of cold electrons. In

contrast to those steady-state measurements, the time evolution of transient carrier distributions can be determined by time-resolved luminescence studies on the femtosecond time scale.

Recently, considerable attention has been given to coherent phenomena connected to the coupling of the initial polarization in the photoexcited semiconductor with an ultrafast laser excitation.[23–29] The loss of phase coherence dominated by elastic as well as inelastic scattering among carriers is found to occur on a femtosecond time scale at densities of the order of 10^{17} cm^{-3}.[23,29]

In this paper we present a combined experimental and theoretical study of carrier thermalization in GaAs and InP. The experiment is based on luminescence up-conversion with a temporal resolution of $\simeq 100$ fs. The theoretical analysis is performed by the MC method. The temporal and spectral evolution of luminescence from GaAs and InP within the first picosecond after excitation at 1.93 eV is measured and simulated for plasma densities between 10^{17} and 7×10^{17} cm^{-3}. Luminescence in a wide range of energies from the band gap up to 1.7 eV exhibits an instantaneous rise within the first 200 fs. The broad structureless spectra observed at these early delay times give evidence of the fast redistribution of Γ valley electrons and holes within 100 fs.

The paper is organized as follows: After a brief description of the experimental method in Sec. II, we present experimental results on GaAs and InP (Sec. III). The data are discussed in a qualitative manner in Sec. IV, whereas the detailed MC calculations of Sec. V give a quantitative analysis of the data. In Sec. VI our experimental findings are compared with other results in the literature. Concluding remarks are given in Sec. VII.

II. EXPERIMENTAL TECHNIQUE

Thin GaAs and InP crystals grown by molecular-beam epitaxy were studied in our measurements. The GaAs sample consists of a 0.6-μm-thick layer clad by $Al_{0.35}Ga_{0.65}As$ layers. The InP layer of a thickness of 2 μm was grown on an InP substrate.

In the time-resolved experiments, the samples are excited by 120-fs pulses at a photon energy of 1.93 eV generated in a mode-locked dye laser with a high repetition rate of 76 MHz. The luminescence is detected by spectrally and temporally resolved up-conversion.[30] The luminescence photons collected by a Cassegrainian mirror optics are mixed with a second laser pulse in a nonlinear $LiIO_3$ crystal (thickness $l=0.5$ mm) to generate the sum frequency. This signal in the ultraviolet is spectrally analyzed by a double monochromator (resolution 5 meV) and detected by single-photon counting.

The time resolution of the experiment is determined by the group-velocity mismatch between the luminescence and the up-conversion pulse in the nonlinear crystal and by the duration of the laser pulses. The first contribution was estimated with the equations given in Ref. 30 and has a value of less than 65 fs for photon energies of the luminescence between 1.45 and 1.93 eV. Thus the duration of the laser pulses of 120 fs represents the limiting factor, resulting in an overall time resolution of approximately 100 fs.

In the following, we present results for various carrier densities in the range between 10^{17} and 7×10^{17} cm^{-3}. The excitation densities are estimated from the absorption coefficient of GaAs and InP at 1.93 eV, the sample thickness, and the spot size of the excitation beam with an accuracy of $\pm50\%$. The values quoted are for the center of the Gaussian excitation profile. The average densities are substantially lower.

III. EXPERIMENTAL RESULTS

Luminescence spectra of GaAs at room temperature which were measured at very early delay times are presented in Fig. 1 for carrier densities of 1.7×10^{17} cm^{-3} (dashed lines) and 7×10^{17} cm^{-3} (solid lines). The well-

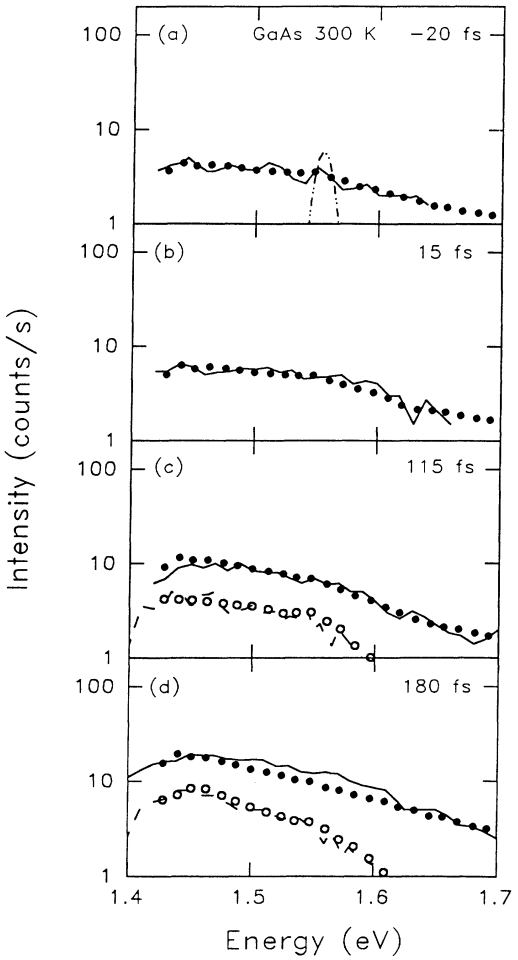

FIG. 1. Luminescence spectra of GaAs observed after femtosecond excitation at 1.93 eV. The excitation density was 7×10^{17} cm^{-3} (solid lines) and 1.7×10^{17} cm^{-3} (dashed lines). The emission intensity is plotted as a function of photon energy for delay times of (a) −20 fs, (b) 15 fs, (c) 115 fs, and (d) 180 fs. The symbols represent the spectra calculated from Monte Carlo simulations using a static multiscreening approach for carrier-carrier scattering. The dash-dotted line in (a) represents a calculated luminescence line originating from the initial electron distribution.

pronounced change of the luminescence intensity and of the shape of the emission bands with time demonstrates the high temporal resolution of our experiments. At all delay times, we find very broad emission spectra covering the energy interval from the band gap at 1.42 up to 1.7 eV. This range is much wider than any structure in the initial nonequilibrium distribution of carriers generated by femtosecond excitation. To illustrate this fact, we have plotted a calculated luminescence line in Fig. 1(a) that is due to the initial electron population created by excitation from the split-off valence band recombining with heavy holes. The spectrally integrated luminescence intensity at a delay time of 180 fs has a value of approximately 15% of the maximum emission intensity observed after 10 ps. It should be noted that broad structureless spectra are also observed for the lower excitation density of 1.7×10^{17} cm^{-3}. The symbols in Fig. 1 represent the results of MC simulations which will be discussed in a later section.

The time evolution of luminescence at several fixed photon energies is plotted in Fig. 2 (solid lines). The emission at 1.575 eV originates from conduction-band states lying very close to those populated by excitation from the split-off band and rises instantaneously with excitation. The luminescence kinetics in Fig. 2(b) that is proportional to the time integral over the excitation pulse convoluted with the up-conversion pulse is used for calibration of delay zero. The emission at all other photon energies investigated shows the same fast rise between -200 and $+200$ fs.

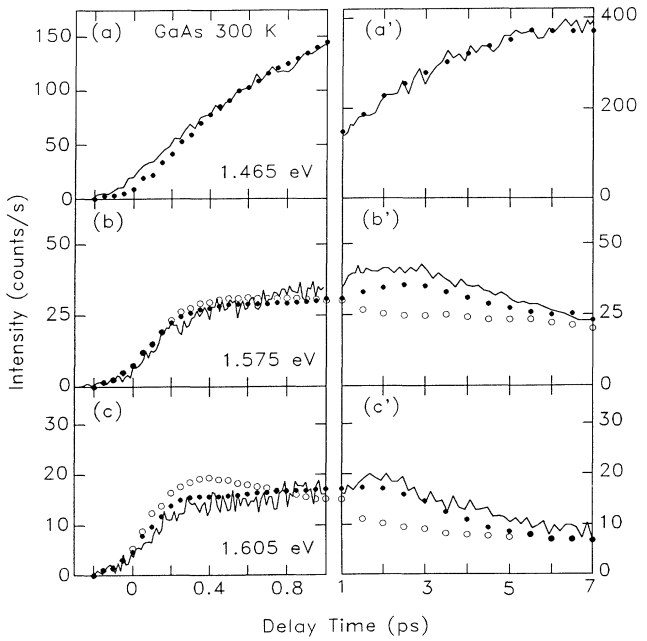

FIG. 2. Femtosecond (left-hand side) and picosecond (right-hand side) time evolution of the luminescence intensity of GaAs at photon energies of (a),(a') 1.465 eV; (b),(b') 1.575 eV; and (c),(c') 1.605 eV (solid lines, excitation density 7×10^{17} cm^{-3}). The symbols give the result of Monte Carlo simulations with an optical deformation potential of $D_{\Gamma-L}=7.5\times10^{8}$ eV/cm (solid circles) and $D_{\Gamma-L}=4\times10^{8}$ eV/cm (open circles).

The femtosecond transients which give direct insight into the fastest scattering processes of the photoexcited carriers are followed by a slower picosecond rise of intensity that is caused by backscattering of electrons from the L and X valleys to the Γ valley and to carrier cooling, the latter process leading to the predominant population of states close to the extrema of valence and conduction bands at long times. The relative strengths of the fast and the slow components of the signal depend on the specific spectral position. Close to the band gap [Fig. 2(a)], the femtosecond component makes up approximately 10% of the intensity occurring after 7 ps, whereas the fast contribution dominates at higher photon energies [Figs. 2(b) and 2(c)]. At energies close to the band gap, the emission intensity reaches its maximum after approximately 10 ps and subsequently decays with the lifetime of the electron-hole plasma on a time scale of several hundreds of picoseconds.

In Fig. 3 we present the emission spectra of InP for delay times of up to 500 fs. In these measurements, the excitation density was 5×10^{17} cm^{-3}. Similar to GaAs, we find broad emission bands at very early times.

Luminescence spectra were recorded up to delay times of 10 ps. In Fig. 4(b) the average carrier energy extracted from the slope of the high-energy tail of the spectra is depicted as a function of delay time (solid circles). The slope is proportional to the product of the distribution

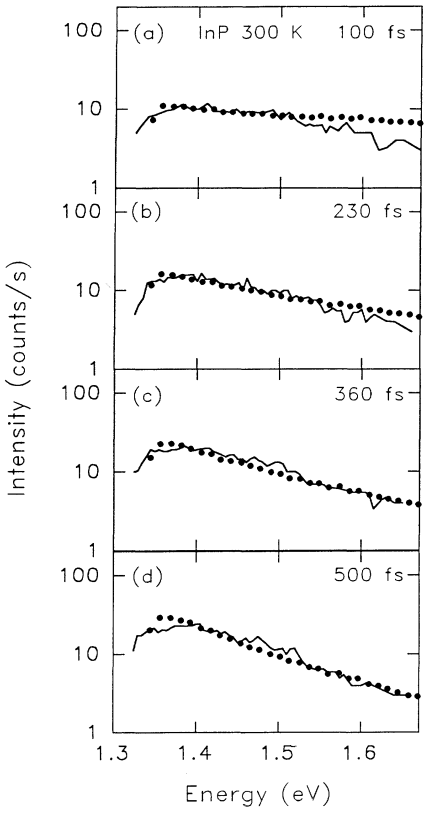

FIG. 3. Emission spectra of InP after femtosecond excitation at 1.93 eV. The excitation density was 5×10^{17} cm^{-3}. The symbols are the results of the numerical simulation.

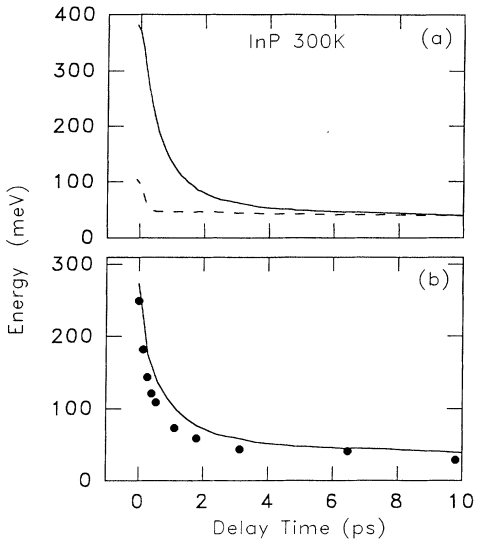

FIG. 4. (a) Average energy of electrons (solid line) and holes (dashed line) in InP as obtained from the Monte Carlo calculations. (b) Average carrier energy derived from the emission spectra as a function of time (solid circles). The solid line represents the results of the Monte Carlo simulations.

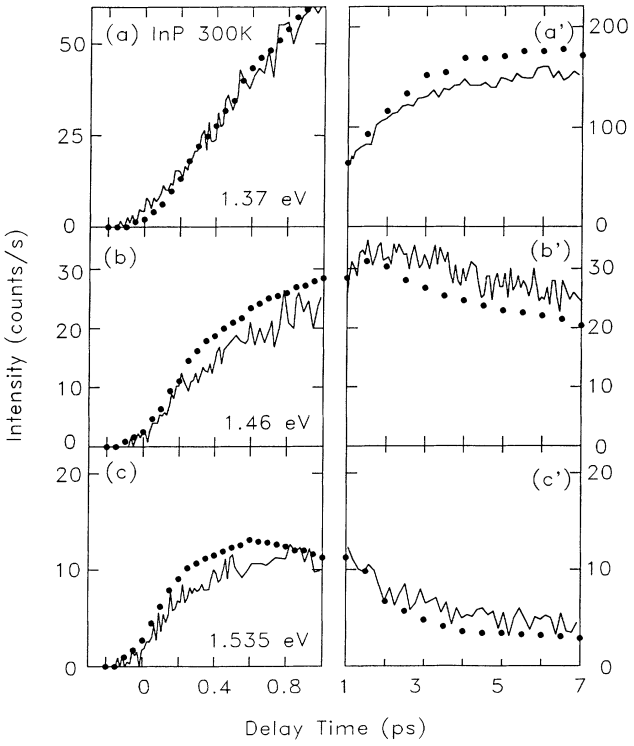

FIG. 5. Femtosecond (left-hand side) and picosecond (right-hand side) kinetics of the luminescence of InP for photon energies of (a),(a') 1.37 eV; (b),(b') 1.46 eV, and (c),(c') 1.535 eV (solid lines, excitation density 5×10^{17} cm^{-3}). The solid circles give the results of Monte Carlo simulations.

function $[f_e(E_c)][f_h(E_v)]$ of electrons and holes at energies $E_{c,v}$ above the respective quasi-Fermi level. For Maxwellian distribution functions, the slope of the high-energy tail in a semilogarithmic plot of intensity versus photon energy is given by $(kT_{\text{eff}})^{-1}$, where k and T_{eff} are Boltzmann's constant and the effective carrier temperature, respectively (see also Sec. V D).

The onset of emission at a number of fixed photon energies is plotted in Fig. 5. We observe a behavior similar to that of GaAs. At high photon energies [Figs. 5(c) and 5(c')], the picosecond component of the signal decays faster than at the corresponding spectral position in GaAs.

IV. DISCUSSION

First, we discuss the relaxation processes of photoexcited carriers in GaAs. Consistent with the findings of our MC simulations, holes thermalize within 100 fs.[9,10] Therefore, recombination with heavy holes dominates the luminescence in the spectral range investigated here because of the larger density of states and larger occupation of the heavy-hole band. At early times (<200 fs), the electrons in the Γ valley come from two sources: (i) electrons excited from the split-off band and (ii) electrons excited from the heavy- and light-hole band that have not been scattered to the L and X valleys. These electrons and holes are created with narrow distributions and thermalize by interacting with other carriers. In addition, they also emit and—with a smaller rate—absorb optical phonons. The large spectral width, the absence of any narrow structures in the spectra (Fig. 1), and the rapid rise of luminescence at all energies (Fig. 2) demonstrate that—for excitation densities between 1.7×10^{17} and 7×10^{17} cm^{-3}—the electrons in the Γ valley and the holes in the heavy-hole band redistribute over a wide energy range within the time resolution of our experiments of 100 fs. The absence of any structure with optical-phonon spacing shows that inelastic carrier-carrier scattering is the main mechanism of thermalization, considerably faster than the LO- or TO-phonon emission times that are longer than 100 fs. The integrated intensity of the GaAs luminescence at 180 fs is 15% of the maximum intensity reached after 10 ps. This fact shows that (1) a large percentage of electrons are in the subsidiary valleys at these early times and (2) practically all electrons in the Γ valley are redistributed over a broad energy range and contribute to luminescence.

It should be noted that luminescence is emitted at photon energies below the band gap of $E_G=1.42$ eV. This behavior is caused by many-body effects strongly influencing the spectral profile of emission around E_G. At present, a quantitative theoretical description of this effect is not available.

In contrast to GaAs, intervalley scattering does not occur in InP for a photon energy of the excitation pulses of 1.93 eV, i.e., the excited electrons reside in the Γ valley for all delay times. The three peaks of the initial electron distribution are located at higher excess energies than in GaAs. Nonetheless, we find no measurable delay in the onset of luminescence originating from states close to the conduction-band minimum (Figs. 3 and 5). This fact un-

derlines the extremely rapid redistribution of the Γ-valley electrons by carrier-carrier scattering.

V. MONTE CARLO SIMULATIONS

A. The Monte Carlo method

We performed a MC simulation of the carrier dynamics using a three-valley Γ, L, and X model for the electrons[7,10] and a three-band scheme for holes.[31,32] The main parameters are listed in Table I. With respect to our previous work,[10,33] we have slightly modified the nonparabolicity factors for the heavy and the light holes, in order to better reproduce the position and intensity of the excitation peaks created by the laser in hot (e,A^0) luminescence studies.[22] In our simulation, electrons are excited from the heavy, light, and split-off hole bands with a ratio of 0.4:0.3:0.3, in good agreement with recent $\mathbf{k}\cdot\mathbf{p}$ calculations[15] accounting for the wave-function overlap between valence- and conduction-band states. Nonequilibrium phonons are included in the simulation.[34] Degeneracy effects have been taken into account both during laser excitation and for all scattering events during the simulation.[37] We include the luminescence arising from recombination of electrons with light holes. The latter is found to make a minor contribution to the spectra, even at very early times. We also investigate the effect of the exciton enhancement by computing the luminescence intensity $I_{\rm lum}(\hbar\omega)$ with the following expression:

$$I_{\rm lum}(\hbar\omega)\propto\frac{G(\hbar\omega)}{1-e^{-2\pi[E_x/(\hbar\omega-E_g)]^{1/2}}}f_e f_h\ , \tag{1}$$

where $G(\hbar\omega)$ is the optical density of states [in first approximation proportional to $(\hbar\omega)^2$], E_x is the exciton binding energy, and E_g is the energy gap (for an overview on the recombination process see, for example, Ref. 35). In our previous work we used the well-known binding energy $E_{ex}=4.4$ meV for GaAs which is the energy for the unperturbed semiconductor. During the laser excitation, as we generate a considerable density of carriers, there is an appreciable band-gap renormalization, and the reduction in the band gap causes a reduction in the exciton binding energy. From a physical point of view, this effect can be interpreted as the screening of the exciton produced by the free electrons and holes.[36] Therefore, we use now a modified value of 2.5 meV for E_x.[29] For a comparison with the experimental results, the calculated spectra and luminescence kinetics are convolved in time with the excitation and the up-conversion pulses.

Monte Carlo methods have been discussed thoroughly in the literature.[37] In the following, we therefore focus on the different schemes used within the MC calculation to treat carrier-carrier (CC) scattering, the scattering process most relevant for the analysis of the present experiments. The main problem relates to screening of the Coulomb interaction. Within the random-phase approximation (RPA), screening depends on the different distribution functions of all types of carriers present in the

TABLE I. Parameters used in the Monte Carlo simulations (m_0 is the free-electron mass).

Parameter	GaAs	InP	Unit
Effective mass m_Γ	0.067	0.075	m_0
m_L	0.222	0.440	
m_X	0.580	0.580	
$m_{\rm hh}$	0.450	0.650	
$m_{\rm lh}$	0.082	0.120	
$m_{\rm soh}$	0.151	0.120	
Nonparabolicity factors Γ	0.612	0.612	$\rm eV^{-1}$
L	0.462	0.462	
X	0.205	0.205	
hh	1.034	1.034	
lh	2.057	2.057	
soh	−0.152	−0.152	
Band-gap energies at $T=300$ K (soh,hh)	0.340	0.110	eV
(hh,Γ)	1.422	1.339	
(Γ,L)	0.285	0.610	
(Γ,X)	0.480	0.760	
Crystal mass density	5.36	4.79	$\rm g/cm^3$
Lattice constant a_0	5.64	5.45	Å
Static dielectric function ϵ_0	12.90	12.35	
High-frequency dielectric function ϵ_∞	10.92	9.52	
LO-phonon energy	35.4	41.7	meV
Intervalley (IV) -phonon energy $\hbar\omega_{\Gamma\to L}$	25.8	39.4	
IV-phonon energy $\hbar\omega_{\Gamma\to X}$	26.4	40.2	
TO-phonon energy	27.8	42.4	
IV-deformation potential $D_{\Gamma\to L}$	7.5	5.0	eV/Å
$D_{\Gamma\to X}$	7.0	5.0	
Hole deformation potential	9.0	9.0	

semiconductor. For a time-dependent situation, as in our investigation, the time evolution of the distributions implies that screening is a dynamical process which in turn modifies the CC interaction. So far, CC scattering has been accounted for via three different approaches: (i) a time-dependent static screening formulation[31] where a single screening length is calculated from RPA in the static limit and updated during the simulation to follow the evolution of the carrier distribution functions, (ii) a generalization of the static screening formalism involving different screening lengths for every carrier population, and (iii) a joint ensemble Monte Carlo molecular-dynamics (EMCMD) approach. Details of the three approaches are given below.

B. Carrier-carrier interaction

The standard approach to study the effect of CC scattering on the transport properties of semiconductors treats the interaction in **k** space using a static screening formulation of the Coulomb interaction potential:

$$V(r)=\frac{e^2}{4\pi\epsilon r}\exp(-r/\lambda_S)\ , \tag{2}$$

where λ_S is the screening length, e the electronic charge, and ϵ the dielectric function of the material. Following the work of Bohm and Pines,[38] this expression is equivalent to considering only the long-wavelength contribution of the Coulomb potential.[31] The other contribution associated to the long-range collective excitations of the electron gas gives rise to plasma oscillations. The actual separation of the two terms must be handled with care since it requires the introduction of a somewhat arbitrary cutoff. In the presence of carriers with different masses and/or different energies (as, e.g., for electrons injected or photoexcited into heavily doped regions), the electron-plasmon interaction constitutes a very effective channel of energy exchange. In the case of laser excitation in intrinsic semiconductors, the separation between single-particle and collective excitations is questionable since these are complementary aspects of the same carrier gas. However, the plasmons are strongly damped[39] and only binary collisions remain if the energy distribution functions are far from equilibrium (as is often the case in ultrafast optical experiments). In this situation, the energy exchange among the hot carriers is quite ineffective. In the following, we will therefore concentrate only on the short-range screened Coulomb interaction. The transition probability of two carriers from wave vectors $\mathbf{k}_1$ and $\mathbf{k}_2$ to $\mathbf{k}_1'$ and $\mathbf{k}_2'$ via the potential of Eq. (2) is obtained from Fermi's golden rule:

$$S_{\mathbf{k}_1,\mathbf{k}_2\rightarrow\mathbf{k}_1',\mathbf{k}_2'}=\frac{2\pi}{\hbar}|M|^2(1-f_{\mathbf{k}_1'})(1-f_{\mathbf{k}_2'})\times\delta(E_{\mathbf{k}_1'}+E_{\mathbf{k}_2'}-E_{\mathbf{k}_1}-E_{\mathbf{k}_2})\ , \tag{3}$$

where

$$M=\langle\mathbf{k}_1,\mathbf{k}_2|V(r)|\mathbf{k}_1',\mathbf{k}_2'\rangle=\frac{e^2}{v\epsilon}\frac{\delta_{\mathbf{k}_1+\mathbf{k}_2,\mathbf{k}_1'+\mathbf{k}_2'}}{|\mathbf{k}_1'-\mathbf{k}_1|^2+\beta^2}\ ,$$

with the crystal volume v and $\beta=1/\lambda_S$. Neglecting degeneracy (which will be accounted for in the simulation via a rejection technique[40]), i.e., assuming $f_{\mathbf{k}_1'}=f_{\mathbf{k}_2'}=0$, the total scattering rate for an electron with wave vector $\mathbf{k}_1$ is obtained by summing over $\mathbf{k}_2,\mathbf{k}_1',\mathbf{k}_2'$ and considering that the probability to find a particle in $\mathbf{k}_2$ is $f_{\mathbf{k}_2}$:

$$\Gamma(\mathbf{k}_1)=\frac{2\pi}{\hbar}\sum_{\mathbf{k}_2}\sum_{\mathbf{k}_1'}\sum_{\mathbf{k}_2'}\left[\frac{e^2}{v\epsilon}\right]^2\frac{\delta_{\mathbf{k}_1+\mathbf{k}_2,\mathbf{k}_1'+\mathbf{k}_2'}}{|\mathbf{k}_1'-\mathbf{k}_1|^2+\beta^2}\times f_{\mathbf{k}_2}\delta(E_{\mathbf{k}_1'}+E_{\mathbf{k}_2'}-E_{\mathbf{k}_1}-E_{\mathbf{k}_2})\ . \tag{4}$$

We define the wave vector exchanged in the scattering as

$$\mathbf{q}=\mathbf{k}_1'-\mathbf{k}_1=\mathbf{k}_2-\mathbf{k}_2'$$

and the relative wave vector as

$$\mathbf{g}=2\mu\left[\frac{\mathbf{k}_1}{m_1}-\frac{\mathbf{k}_2}{m_2}\right]\ ,$$

where μ is the reduced mass of the two carrier masses m_1 and m_2. Equation (4) can be written as

$$\Gamma(\mathbf{k}_1)=\frac{e^4}{4\pi^2\epsilon^2 v\hbar}\sum_{\mathbf{k}_2}f_{\mathbf{k}_2}\int d\mathbf{q}\frac{\delta\left[\frac{\hbar^2q^2}{2\mu}+\frac{\hbar^2}{2\mu}qg\cos\xi\right]}{q^2+\beta^2}\ ,$$

where ξ is the angle between $\mathbf{q}$ and $\mathbf{g}$. Performing the integration, we obtain

$$\Gamma(\mathbf{k}_1)=\frac{\mu e^4}{2\pi\epsilon^2 v\hbar^3}\sum_{\mathbf{k}_2}f_{\mathbf{k}_2}\frac{|\mathbf{g}|}{\beta^2(\mathbf{g}^2+\beta^2)}\ . \tag{5}$$

The sum over the distribution function of the partner electron is indeed an ensemble average, i.e., a sum over all the particles that is easy to compute in a MC simulation. Thus we have

$$\Gamma(\mathbf{k}_1)=\frac{ne^4}{2\pi\epsilon^2\hbar^3\beta^2N}\sum_{i=1}^{N}\frac{2\mu_i^2\left|\frac{\mathbf{k}_1}{m_1}-\frac{\mathbf{k}(i)}{m_i}\right|}{4\mu_i^2\left|\frac{\mathbf{k}_1}{m_1}-\frac{\mathbf{k}(i)}{m_i}\right|^2+\beta^2}\ , \tag{6}$$

where N is the number of simulated particles. Equation (6) describes the probability for an electron with wave vector $\mathbf{k}_1$ to interact with all other carriers of the ensemble. Obviously, by performing the sum over carriers of a given type (for instance, heavy holes or L-valley electrons), it is possible to calculate the rate relative to only this type of carriers.

The inverse screening length β plays a fundamental role in the carrier-carrier interaction. It was shown in Ref. 31 that—starting from the dielectric function within the random-phase approximation and taking the small wave-vector limit—it is possible to compute this quantity using a self-consistent method which takes into account the time evolution of the carrier distribution function:

$$\beta^2=\frac{e^2}{\epsilon}\int\left[-\frac{\partial f(E)}{\partial E}\right]D(E)dE\ , \tag{7}$$

where $D(E)$ is the density of states. This expression simplifies for parabolic bands (carrier-carrier scattering is always treated in this approximation because of the difficulties in handling the energy-conserving δ function for nonparabolic dispersion) to

$$\beta^2=\frac{ne^2}{2\epsilon}\frac{1}{N}\sum_i\frac{1}{E_i}\ . \tag{8}$$

In the limit of a Maxwellian distribution, this formula gives the well-known Debye screening length. From a physical point of view, the quantity β represents the fact that carriers are screening each other; larger β implies stronger screening and therefore reduced scattering rates. As we will discuss in connection with the actual simulation of ultrafast spectroscopy, the comparison of our simulation with the EMCMD to be discussed in Sec. V C gives us the possibility of determining the effect of the static-screening assumption, its limitations, and its possible improvements. The heaviest carriers, i.e., heavy holes and electrons in the upper valleys, have the lowest average energy and make—in the static limit—the main contribution to the screening, strongly reducing the scattering rates of all carriers. This is somehow unphysical, because one expects the heavier particles not to be able to move fast and screen the mutual interaction of light carriers. The origin of this problem lies in the static-screening approximation, i.e., if only small values of $\mathbf{q}$ are considered for $\omega=0$, all dynamical information about the system is lost. With an intuitive approach, we can reintroduce the dynamical properties of the system by considering not only one single screening length for the entire system, but many different screening lengths, one for each carrier population, that is, electrons in the Γ, L, and X valleys as well as holes in the three valence bands.[41] In this case, the scattering rate and the selection of the final states for a particle that belongs to a carrier population labeled with the index i interacting with a particle with the same or lighter mass are computed starting from the following expression for the inverse of the screening length:

$$\beta_i^2=\frac{n'e^2}{2\epsilon}\frac{1}{N'}\sum_j{}'\frac{1}{2E_j}\ , \tag{9}$$

where the primed sum means that we are summing over all the particles such that $m_j\le m_i$, and n' and N' are, respectively, the density and the number of this subensemble of carriers. In this case, for example, electrons in the Γ valley are screened only by themselves, and this results in a much higher scattering rate for them. We will show that this approach greatly improves the results obtained with the static-screening model and gives almost the same scattering dynamics as the full MD method that is much more time consuming.

Recent work has shown that the static-screening approximation can be overcome and dynamical screening can be implemented.[42–44] However, such an approach requires huge computational time that cannot be afforded in present Monte Carlo simulations. In contrast, the static-screening formalism presented so far lends itself quite naturally to the incorporation into Monte Carlo codes. Different implementations of the method have been presented and critically discussed in Ref. 45. In our calculations, we tabulate the carrier-carrier scattering rate calculated from Eq. (6) and update it at fixed times during the simulation, as was discussed in Refs. 33 and 34. When an electron is selected, a partner electron is chosen from the ensemble. Then, the final states of the two electrons after the scattering are obtained from the differential scattering probability. Since this criterion forces the partner electron to scatter independently from its own scattering rate, the total tabulated rate is actually divided by 2 in order to balance this overestimation. It should be noticed that all the different methods examined in Ref. 45 for the partner selection give no significant differences when applied to the study of carrier relaxation following photoexcitation.

C. The molecular-dynamics approach

The main limitations of the static-screening approach are (i) the assumption of the same screening length for all particles, calculated as a mean value on the ensemble, and (ii) the assumption that the many-body interaction can be separated into binary collision and plasmon scattering events.

As shown above, the first assumption can be partially avoided by computing a separate screening length for each individual type of carrier present in the ensemble. Although still based on the assumption of linear screening and although fluctuations in the actual interparticle scattering process are neglected, this correction will be shown to improve substantially the description of ultrafast phenomena where carrier-carrier scattering is important. In the following, this method will be referred to as the "static multiscreening" (SMS) method.

All assumptions can be avoided with the use of an alternative method for the treatment of the carrier-carrier interaction that has been proposed originally by Jacoboni (the method is described in Ref. 37). It is based on a molecular dynamics (MD) simulation for the real-space trajectories of the ensemble of carriers interacting via the bare Coulomb potential, coupled to the standard EMC algorithm for the $\mathbf{k}$-space dynamics. The strength of the method lies in the fact that it does not require any assumptions on the screening between carriers. Furthermore, it accounts for a fundamental property of a classical electron gas, the carrier density fluctuations.[40,46] The main extension with respect to the traditional EMC routine is found in the splitting of the free flights between scattering events, in order to account properly for the changes in the interparticle Coulomb forces as the electrons move in the system. The classical equations of motion are solved within a finite difference scheme by using a discretization time step δt. During each step, each carrier is subject to the Coulombic force originating from all other carriers. There are two main problems in this real-space simulation: (i) the amplitude of the time step δt and (ii) the boundary conditions imposed on the system

which is dominated by long-range Coulomb forces.

The choice of δt is of fundamental importance in order to have an accurate simulation of the system. If δt is very small, the electron trajectories are reproduced with small errors, but unaffordable computer time is required. On the contrary, a δt that is too large will result in a large error of the simulated trajectories. This deficiency will in turn lead to an erroneous evaluation of the potential and kinetic energy of the system, altering the results of the whole simulation. We have found that a good value for δt is determined by half the ratio of the minimum distance and the maximum velocity within the ensemble of carriers. This choice of δt ensures that even in the most unfavorable case where the two closest carriers would move against each other with the highest velocity, the δt would be such that it would not allow the crossing of the trajectories.

The problem of the long range of the Coulomb interaction can be solved by implementing periodic boundary conditions. The simulation cubic box (with a volume determined by the ratio of the number of simulated particles divided by the density they represent) is replicated throughout space to form an infinite lattice. During the simulation, as a particle moves into the original box, its periodic image in each of the neighboring boxes moves exactly in the same way. So, when a carrier leaves the central box, one of its images enters through the opposite face of the box. In this way, there are no artificial boundaries introduced in the simulation. A problem might arise from the fact that the use of periodic boundary conditions inhibits the occurrence of long-wavelength fluctuations, i.e., if L is the length of the cube, every fluctuation with wavelength greater than L is suppressed. Fortunately, even if the potential is long range, carriers do actually screen each other, and we have verified that usually when two carriers are more than five mean distances apart, they only marginally feel the reciprocal interaction. This requires, in order to perform a correct simulation, consideration of at least 1000 particles. In this way, every carrier can be considered as the center of a box with, on the average, 10 particles on each side.

Let us focus on the method for computing the intercarrier forces. In order to maintain the neutrality of the system, usually a uniform background is added. To compute the force acting on the ith particle, we must sum the force created by the background and by all other $N-1$ particles, including in principle the contribution from the image boxes. As an alternative, we have implemented a simple algorithm on the basis of which each particle is placed at the center of a virtual box and only the contribution of the other particles contained in such a box are considered. In this way, the background does not have to be considered (since its effect at the center of the box is zero).

D. Numerical results

The symbols in Fig. 1 are the results of MC simulations using the SMS method. Good agreement with the data is found for both excitation densities. In particular, the calculation reproduces the very fast broadening of the initial peaks in the carrier distribution functions. As pointed out earlier, excitons should be screened at these densities. In fact, we obtain the best fit to the experiments using a binding energy of 2.0 meV and such a value is in good agreement with preliminary results in Ref. 29 which show—for an excitation density of 7×10^{17} cm^{-3}—a band-gap renormalization of 2.5 meV when the carriers are excited far from the band gap. In Fig. 6 we present spectra for a delay time of 15 fs which were computed with the different approaches to treating carrier-carrier scattering. The simulation performed with different screening lengths for each individual type of carrier (solid line) compares well with the more general molecular-dynamics scheme (dotted line) that has been shown to include all the features of dynamical screening.[40] Such an approach also incorporates the collective components of a Coulombic plasma,[33] reproducing experimental situations where plasmon losses are important.[21] The spectrum obtained with the standard static-screening approximation (dashed line) is different, presenting a maximum at the energy corresponding to split-off excitation. This finding underlines the fact that this treatment of carrier-carrier scattering underestimates the overall interaction strength, i.e., it overestimates the screening. It should be pointed out that the three methods give different results only for delay times shorter than 200 fs, whereas at later times the distribution functions are in all cases almost Maxwellian.

The time evolution of luminescence calculated with the multistatic screening approach is plotted in Fig. 2 for three photon energies (symbols). The rapid onset of emission at the different spectral positions, which is indicative of the ultrafast redistribution of electrons and holes, is well reproduced by the simulation. The luminescence intensity at higher photon energies [Figs. 2(b) and 2(c)] shows a maximum after 2 to 3 ps that is due to an increase of (electron) population in the optically coupled states of the Γ valley. (At these times, holes are almost completely in equilibrium with the lattice.) Those elec-

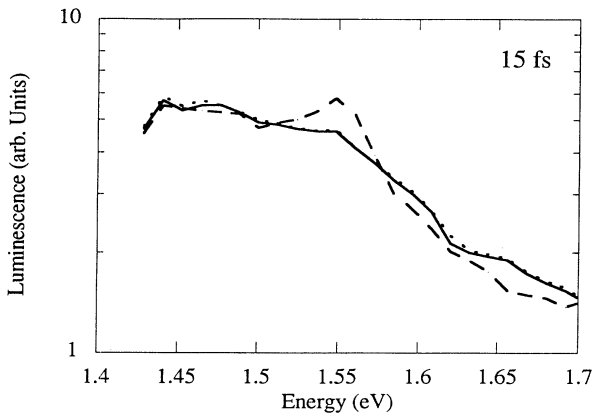

FIG. 6. Emission spectra of GaAs at a delay time of 15 fs computed by the Monte Carlo method with the three different approaches to treat carrier-carrier scattering: molecular dynamics (dotted line), static screening (dashed line), and static multiscreening (solid line, excitation density 7×10^{17} cm^{-3}).

trons are provided by the picosecond backscattering from the L and X valleys. The rate at which electrons reenter from the upper valleys is higher than the rate at which they leave the high-energy region of the Γ valley. Correspondingly, the calculated time evolution is sensitive to changes of the deformation potential $D_{\Gamma L}$ that governs intervalley scattering. To study the effect more quantitatively, we have compared the results obtained using a value of $D_{\Gamma L}=7.5\times10^8$ eV/cm (which is the value that reproduces the experimental results very well; solid circles in Fig. 2) with those of a simulation where $D_{\Gamma L}=4\times10^8$ eV/cm (open circles). We emphasize that in our simulation a single effective intervalley phonon contributes to intervalley scattering via the $D_{\Gamma L}$ coupling constant. As pointed out in Ref. 47, the actual intervalley process results from the contribution of acoustic as well as optical phonons. For the smaller coupling (open circles in Fig. 2) we notice that—after a fast initial rise—the luminescence intensity exhibits a sharper decrease with respect to the higher coupling, in disagreement with the experimental data. This behavior can be understood from Fig. 7 where we show the relative population in the Γ and L valleys as a function of time delay for the two coupling constants. The stronger coupling (solid lines) favors the transition to the satellite valleys with the population reaching its maximum after about 400 fs. At longer times, also, the return into the Γ valley is enhanced. Conversely, with the lower constant (dotted lines), the maximum population in L reaches a lower value at a later time (750 fs). Also, the rate at which electrons reenter the Γ valley is much lower, and so it does not reproduce the experimental intensities.

In Fig. 8 we show the energy distribution function of electrons at times of 0, 100, and 200 fs over an energy range that includes the three excitation peaks, using EMC-SMS. The results in Fig. 8 are not convolved with the time envelope of the laser pulses. The initial maxima

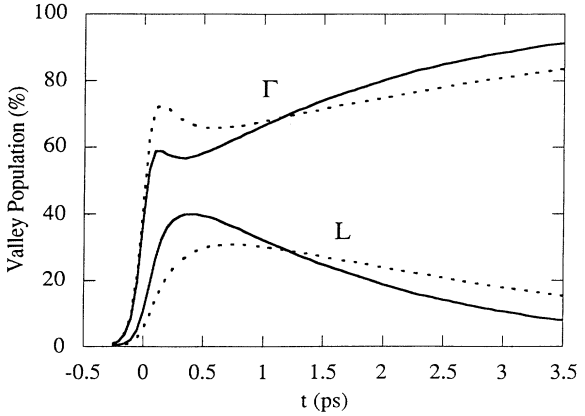

FIG. 7. Relative electron populations of the Γ and L valleys of GaAs as calculated from the Monte Carlo method. The overall population generated by femtosecond excitation at 1.93 eV (final carrier density 7×10^{17} cm^{-3}) is plotted as a function of time for two values of the optical deformation potential $D_{\Gamma-L}$ governing the rate of intervalley scattering. Solid line, $D_{\Gamma-L}=7.5\times10^8$ eV/cm; dashed line, $D_{\Gamma-L}=4\times10^8$ eV/cm.

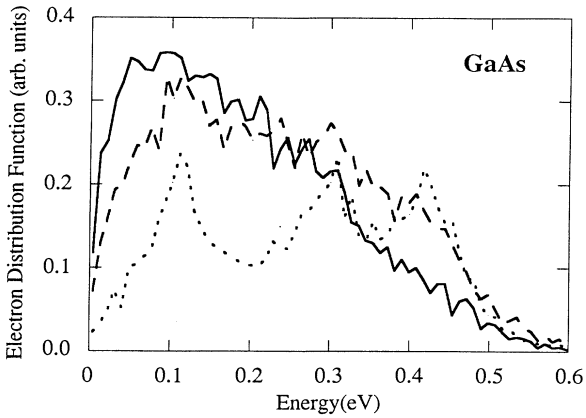

FIG. 8. Electron distribution function in the Γ valley of GaAs calculated for delay times of 0 fs (dotted line), 100 fs (dashed line), and 200 fs (solid line, carrier density 7×10^{17} cm^{-3}).

of electron population are clearly seen at $t=0$ fs, whereas after 100 fs, the distribution is already completely broadened. This finding is due to the very effective carrier-carrier scattering occurring on a time scale considerably faster than the average carrier-phonon scattering times. This is confirmed by the results presented in Figs. 9 and 10. In Fig. 9 we have plotted the percentage of electrons in the L valley originating from the three excitation peaks normalized to the total number of electrons in each peak. The dotted line represents the probability of finding an electron generated from the split-off band, i.e., about 200 meV below the threshold for the scattering to L, in the L valley. The probability reaches a value of about 12%, showing that it is indeed possible to find electrons excited from the split-off band at high energy. This fact demonstrates that the internal thermalization produced by CC scattering is actually faster than any type of phonon scattering. This is further illustrated by Fig. 10 where we have plotted the total kinetic energy exchanged by the electrons in the Γ valley. The solid curve

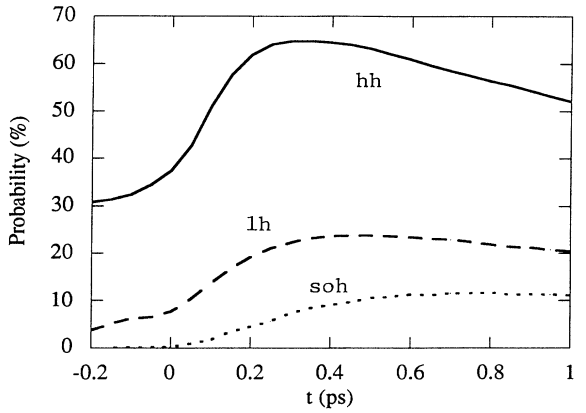

FIG. 9. Time variation of the percentage of electrons in the L valley of GaAs generated originally from the split-off (dotted line), light-hole (dashed line), and heavy-hole (solid line) valence bands (excitation density 7×10^{17} cm^{-3}).

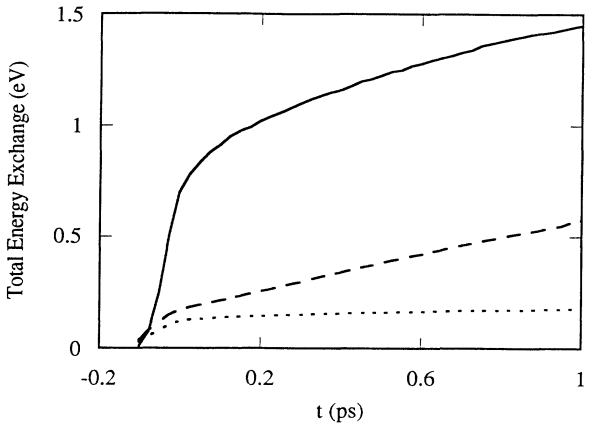

FIG. 10. Total energy exchanged by the electrons in the Γ valley in GaAs. The solid line represents the contribution of all carrier-carrier scattering mechanisms; the dashed and dotted lines represent, respectively, the contribution of polar and nonpolar (intervalley) optical phonons.

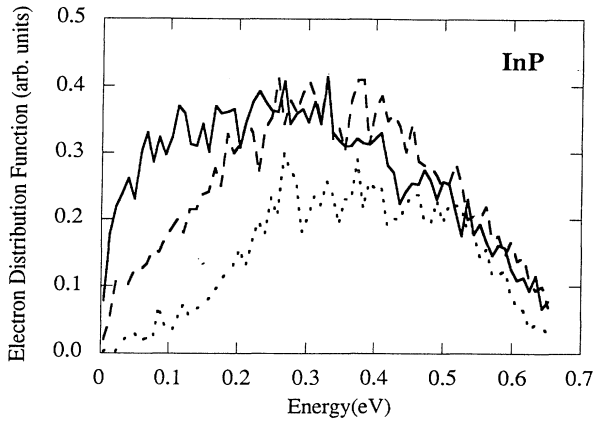

FIG. 11. Electron distribution function in the Γ valley of InP calculated for delay times of 0 fs (dotted line), 100 fs (dashed line), and 200 fs (solid line).

represents the energy exchanged with CC scattering and is much larger than that exchanged with the polar optical phonons (dashed line) and with the equivalent intervalley nonpolar optical phonon (dotted line).

Similar results have been obtained in the simulation of the carrier dynamics in InP. Due to the smaller band gap and the smaller split-off separation of InP, electrons are generated in the Γ valley with a much larger excess energy. In fact, the excitation peak coming from the split-off band is found 260 meV above the bottom of the Γ valley. For photoexcitation around 2 eV, very few electrons transfer from the Γ valley to the L and X minima of the conduction band, which lie substantially higher than in GaAs. As a result, the L and X electrons scattered back to the Γ valley on a picosecond time scale make a negligible contribution to the luminescence kinetics at high photon energies [cf. Figs. 5(c) and 5(c')] that decays faster than in GaAs.

Experimental data and theoretical curves for InP are compared in Figs. 3, 4, and 5 and show good agreement. The substantial increase of the band-edge luminescence at zero time delay is a clear indication of an extremely efficient redistribution caused by carrier-carrier scattering, combined with an equally fast hole relaxation. This behavior is also evident from the electron distribution functions in InP that are plotted in Fig. 11 at times of 0, 100, and 200 fs and from a comparison to the corresponding distributions for GaAs (Fig. 8). In particular, the original excitation peaks in InP have disappeared in the distribution functions at time $t=0$. Once again, the stronger thermalization effect in InP can be attributed to the energy dependence of the screening length. The presence of carriers with higher kinetic energy results in a smaller β, i.e., a higher scattering rate.

A small discrepancy between the experimental and theoretical results is observed in the luminescence spectra of Fig. 3. At very early times, the experimental spectra show a cooler system. As mentioned above, the transfer to the upper valleys is negligible in InP, and the cooling of electrons can only proceed through the emission of polar optical phonons whose scattering rate is already well known and accepted. The mechanism that could be responsible for such enhanced cooling is the electron-hole interaction. It is possible that our treatment of this scattering in the presence of a large number of high-energy carriers (as in InP) is still insufficient to account fully for the experimental results (in GaAs, the high-energy carriers are quickly transferred to the upper valley so they lose most of their kinetic energy).

In Fig. 4(a) we present the calculated mean energy of Γ-valley electrons and of heavy holes as a function of time. Using this information, we calculate an effective mean energy of the electron-hole plasma which is compared in Fig. 4(b) with the values derived from the high-energy tail of the experimental spectra (solid circles). The small discrepancies are mainly due to the fact that the values derived from the experiment are influenced by the (energy-dependent) joint density of states, giving a slightly modified shape of the spectra.

In the present EMC simulations, the coherent coupling of the initial polarization in the semiconductor to the femtosecond excitation pulse is not explicitly taken into account. The fast dephasing of the excited interband transitions may be characterized by a dephasing time T_2 that has—according to photon echo measurements at 2 eV (Ref. 23)—a value of roughly 30 fs for a carrier density of 7×10^{17} cm^{-3}, i.e., short compared to the duration of our excitation pulses of 120 fs. The rapid dephasing results in an additional homogeneous broadening of the optical transitions by approximately 45 meV. Consequently, luminescence originating from the initial nonequilibrium distribution of carriers that is generated by femtosecond excitation would exhibit three peaks of a width determined by the laser bandwidth, the warping of the band structure, and the homogeneous broadening. It is important to note that the spectra we observed at early delay times [cf. Figs. 1(a) and 1(b)] are substantially broader than any structure related to those initial nonequilibrium populations, giving evidence of the ultrafast redistribution of the carriers. Nonetheless, investigation of the influence of coherent phenomena on the luminescence observed at very early delay times would be in-

teresting[27–29] and simulations of those effects by extended Monte Carlo techniques are presently under way.[29]

VI. COMPARISON WITH OTHER EXPERIMENTS

We now compare our results to other investigations of subpicosecond carrier relaxation photoexcited around 2 eV. Femtosecond nonlinear absorption studied between 1.57 and 2.15 eV (Refs. 2 and 3) could not provide unambiguous information on carrier thermalization, as discussed earlier. Dephasing of a coherent polarization by carrier-carrier scattering has been investigated in photon-echo experiments with pulses of a duration of 6 fs.[23] The dephasing times of 12 to 45 fs reported for carrier densities between 7×10^{18} and 1.5×10^{17} cm^{-3} are not in contradiction with our results since coherence can be broken by purely elastic collisions which do not lead to thermalization. Thermalization of a nonequilibrium distribution generated by optical excitation at 2 eV has been simulated by EMC calculations with carrier densities between 10^{17} and 10^{18} cm^{-3}.[7,14–16,31,33] Assuming a statically screened carrier-carrier interaction, the holes were found to thermalize within the first 100 fs, whereas the electrons equilibrate much slower. Such slow electron relaxation would result in structured luminescence spectra at early times and can be ruled out from our luminescence data, directly showing the rapid population of electronic states over a wide energy interval. We have shown that the previous discrepancy between experiments and Monte Carlo simulation lies mainly in the static-screening approximation which does not fully account for the carrier-carrier scattering in far-from-equilibrium situations. Also, the thermalization time of 180 fs obtained for a hot low-density (2×10^{15} cm^{-3}) electron gas in the presence of a cold electron-hole plasma of high density (8×10^{16} cm^{-3}) cannot be directly compared with our faster thermalization times because of different experimental conditions.[21] The results of Ref. 33 obtained with exactly the same parameters and the same MC program used here show that there is not any contradiction in these different findings. The physical reason for this difference can be attributed to two effects: first, as shown in Eq. (8) and also in the different results obtained for GaAs and InP, the screening length is inversely proportional to the energy of the carriers, so the presence of a cold electron-hole plasma strongly reduces the carrier-carrier interaction. Second, plasmon losses that are relevant in the situation of Refs. 21 and 33 are almost completely absent in the room-temperature upconversion experiment, as confirmed by the fact that we obtained no difference in the calculated carrier dynamics if we include plasmons in our simulations. This finding represents further evidence that carrier-carrier scattering cannot be considered to be dependent only on the carrier density. In some situations, quantities like carrier effective masses and energy are more relevant for screening than the bare density.

Very recently, nonthermal electron distributions close to the Γ minimum of GaAs have been observed in picosecond luminescence studies at excitation densities around 4×10^{13} cm^{-3}.[11] A cross section of 6×10^{-12} cm^2 for electron-electron collisions has been derived from the data showing the formation of a thermal distribution on a time scale of 50 ps. As discussed in Ref. 11, extrapolation of those numbers to the density regime studied in our present experiment gives thermalization times well below 100 fs, consistent with the results reported here.

VII. CONCLUSIONS

In conclusion, the results presented here give direct insight into the initial relaxation of electrons in the central (Γ) valley of GaAs and InP. Femtosecond luminescence spectroscopy reveals the redistribution of electrons and holes over a wide energy range within the first 100 fs after excitation, demonstrating the dominant role of carrier-carrier scattering for equilibration. Comparison with Monte Carlo simulations shows that the inelastic carrier-carrier scattering rates during the first 100 fs are higher than calculated with a statically screened carrier-carrier interaction. In contrast, Monte Carlo calculations including dynamical screening via a molecular-dynamics approach as well as a novel multistatic screening approximation properly describe the experimental results.

[1]C. V. Shank, R. L. Fork, R. F. Leheny, and J. Shah, Phys. Rev. Lett. **42**, 112 (1979).
[2]D. J. Erskine, A. J. Taylor, and C. L. Tang, Appl. Phys. Lett. **45**, 54 (1984).
[3]W. Z. Lin, R. W. Schoenlein, J. G. Fujimoto, and E. P. Ippen, IEEE J. Quantum Electron. **24**, 267 (1988).
[4]J. L. Oudar, D. Hulin, A. Migus, A. Antonetti, and F. Alexandre, Phys. Rev. Lett. **55**, 2074 (1985).
[5]W. H. Knox, C. Hirlimann, D. A. B. Miller, J. Shah, D. S. Chemla, and C. V. Shank, Phys. Rev. Lett. **56**, 1191 (1986).
[6]J. P. Foing, D. Hulin, M. Joffre, M. K. Jackson, J. L. Oudar, C. Tanguy, and M. Combescot, Phys. Rev. Lett. **68**, 110 (1992).
[7]J. Shah, B. Deveaud, T. C. Damen, W. T. Tsang, A. C. Gossard, and P. Lugli, Phys. Rev. Lett. **59**, 2222 (1987).
[8]X. Q. Zhou, G. C. Cho, U. Lemmer, W. Kütt, K. Wolter, and H. Kurz, Solid-State Electron. **32**, 1591 (1989).
[9]X. Q. Zhou, K. Leo, and H. Kurz, Phys. Rev. B **45**, 3886 (1992).
[10]T. Elsaesser, J. Shah, L. Rota, and P. Lugli, Phys. Rev. Lett. **66**, 1757 (1991).
[11]D. W. Snoke, W. W. Rühle, Y.-C. Lu, and E. Bauser, Phys. Rev. Lett. **68**, 990 (1992); Phys. Rev. B **45**, 10 979 (1992).
[12]J. Nunnenkamp, J. H. Collet, J. Klebniczki, J. Kuhl, and K. Ploog, Phys. Rev. B **43**, 14 047 (1991).
[13]T. Gong, P. M. Fauchet, J. F. Young, and P. J. Kelly, Phys. Rev. B **44**, 6542 (1991).
[14]C. J. Stanton, D. W. Bailey, and K. Hess, IEEE J. Quantum Electron. **24**, 1614 (1988).
[15]C. J. Stanton, D. W. Bailey, and K. Hess, Phys. Rev. Lett. **65**, 231 (1990).
[16]X. Q. Zhou and T. Y. Hsiang, J. Appl. Phys. **67**, 7399 (1990).
[17]D. K. Ferry, A. M. Kriman, H. Hida, and S. Yamaguchi, Phys. Rev. Lett. **67**, 633 (1991).
[18]W. Pötz and P. Kocevar, Phys. Rev. B **28**, 7040 (1983).

[19]P. Lugli, P. Bordone, L. Reggiani, M. Rieger, P. Kocevar, and S. M. Goodnick, Phys. Rev. B **39**, 7852 (1989), and references therein.
[20]K. Leo, W. W. Rühle, H. J. Queisser, and K. Ploog, Phys. Rev. B **37**, 7121 (1988).
[21]J. Kash, Phys. Rev. B **40**, 3455 (1989).
[22]G. Fasol, W. Hackenberg, H. P. Hughes, K. Ploog, E. Bauser, and H. Kano, Phys. Rev. B **41**, 1461 (1990).
[23]P. C. Becker, H. L. Fragnito, C. H. BritoCruz, R. L. Fork, J. E. Cunningham, J. E. Henry, and C. V. Shank, Phys. Rev. Lett. **61**, 1647 (1988).
[24]A. Honold, L. Schultheis, J. Kuhl, and C. W. Tu, Appl. Phys. Lett. **52**, 2105 (1988).
[25]E. O. Göbel, K. Leo, T. C. Damen, J. Shah, S. Schmitt-Rink, W. Schäfer, J. F. Müller, and K. Köhler, Phys. Rev. Lett. **64**, 1801 (1990).
[26]D. S. Kim, J. Shah, J. E. Cunningham, T. C. Damen, S. Schmitt-Rink, and W. Schaefer, Phys. Rev. Lett. **68**, 2838 (1992).
[27]G. Böhne, T. Sure, R. G. Ulbrich, and W. Schäfer, Phys. Rev. B **41**, 7549 (1990).
[28]R. Zimmermann, Phys. Status Solidi B **159**, 317 (1990).
[29]T. Kuhn and F. Rossi, Phys. Rev. Lett. **69**, 977 (1992).
[30]J. Shah, IEEE J. Quantum Electron. **24**, 276 (1988).
[31]M. A. Osman and D. K. Ferry, Phys. Rev. B **36**, 6018 (1987).
[32]L. Rota, P. Lugli, T. Elsaesser, and J. Shah (unpublished).
[33]L. Rota, P. Poli, C. Jacoboni, and P. Lugli, in *Proceedings of the Twentieth International Conference on the Physics of Semiconductors,* edited by E. Anastassakis and J. D. Joannopoulos (World Scientific, Singapore, 1990), p. 2534.
[34]P. Lugli, Solid-State Electron. **31**, 667 (1988).
[35]H. Barry Bebb and E. W. Williams, in *Semiconductor and Semimetals,* edited by R. K. Willardson and A. C. Beer (Academic, New York, 1972), Vol. 8, p. 182.
[36]W. F. Brinkman and P. A. Lee, Phys. Rev. Lett. **31**, 237 (1973).
[37]C. Jacoboni and P. Lugli, *The Monte Carlo Method for Semiconductor Device Simulation* (Springer-Verlag, Berlin, 1989), and references therein.
[38]D. Bohm and D. Pines, Phys. Rev. **92**, 609 (1953).
[39]H. Sato and Y. Hori, Phys. Rev. B **36**, 6033 (1987).
[40]P. Lugli and D. K. Ferry, Phys. Rev. Lett. **56**, 1295 (1986).
[41]U. Hohenester, P. Supancic, P. Kocevar, X. Q. Zhou, U. Lemmer, G. C. Cho, W. Kütt, and H. Kurz, Semicond. Sci. Technol. **7**, B176 (1992).
[42]J. F. Young, N. L. Henry, and P. J. Kelly, Solid-State Electron. **32**, 1567 (1989).
[43]R. Binder, D. Scott, A. E. Paul, M. Lindberg, K. Henneberger, and S. W. Koch, Phys. Rev. B **45**, 1107 (1992).
[44]D. C. Scott, R. Binder, and S. W. Koch, Phys. Rev. Lett. **69**, 347 (1992).
[45]M. Mosko and A. Moskova, Phys. Rev. B **44**, 10 794 (1991).
[46]P. Lugli and L. Reggiani, in *Noise in Physical Systems and 1/f Noise,* edited by A. D'Amico and P. Mazzetti (Elsevier, Amsterdam, 1986), p. 235.
[47]S. Zollner, S. Gopalan, and M. Cardona, Phys. Rev. B **44**, 13 446 (1991).